A Study of the Diffusion and Rise of Stack Plumes at Coastal Region by Using LIDAR Observation Data

Ill-Hee Yoon

Department of Earth Science, Kyungpook National University,
Taegu, 702-701, Korea

(Manuscript received 19 November, 1998)

Abstract

The Kwinana Shoreline Fumigation Experiment (KSFE) took place at Fremantle, WA, Australia between January 23 and February 8, 1995. The CSIRO DAR LIDAR measured plume sections from near the Kwinana Power Station (KPS) stacks to up to about 5 km downstream. It also measured boundary layer aerosols and the structure of the boundary layer on some occasions. Both stages A and C of KPS were used as tracers at different times.

The heart of the LIDAR system is a Neodymium-doped Yttrium-aluminum-garnet (Nd:YAG) laser operating at a fundamental wavelength of 1064 nm, with harmonics of 532 nm and 355 nm. For these experiments the third harmonic was used because the UV wavelength at 355 nm is eye safe beyond about 50 m. The laser fires a pulse of light 6 ns in duration (about 1.8 m long) and with an energy (at the third harmonic) of about 70 mJ. This pulse subsequently scattered and absorbed by both air molecules and particles in the atmosphere. A small fraction of the laser beam is scattered back to the LIDAR, collected by a telescope and detected by a photo-multiplier tube. The intensity of the signal as a function of time is a measure of the particle concentration as a function of distance along the line of the laser shot.

The smoke plume was clearly identifiable in the scans both before and after fumigation in the thermal internal boundary layer (TIBL). Both power station plumes were detected. Over the 9 days of operation, 1,568 plumes scans (214 series) were performed. Essentially all of these will provide instantaneous plume heights and widths, and there are many periods of continuous operation over several hours when it should be possible to compile hourly average plume statistics as well. The results of four days LIDAR observations of the dispersion of smoke plume in the TIBL at a coastal site are presented for the case of stages A and C.

1. INTRODUCTION

The Kwinana Shoreline Fumigation Experiment (KSFE) took place at Fremantle, WA, Australia between January 23 and February 8, 1995. The CSIRO DAR LIDAR measured plume sections from near the Kwinana Power Station (KPS) stacks to up to about 5 km downstream. It also measured boundary layer aerosols and the structure of the boundary layer on some occasions.

Kwinana Power Station consists of three Stages. Stage A has been proposed as the base-load unit, operating steadily on coal at an output of 216 MW twenty four hours a day. Its output can be increased by switching to gas or oil, or by supplementing coal with these alternatives. It is proposed to operate Stage B as a peak-load unit running on gas as required. While Stage C can operate on any of the fuels, the boilers experience fouling problems on coal and a coal/gas mix is preferred (Manins, 1990). Both Stages A and C of KPS, however, were used as tracers at different times. The parameters for KPS are listed in Table 1.

Table 1. Parameters for Kwinana Power Station

Stage	Stack Height(m)	Stack Inner Diameter(m)	Preferred Fuels (in order)	Electrical O/P(MW)
A	114.3	4.27	Coal, Gas, Oil	216 - 240
C	189.0	5.33	Gas, Coal, Oil	240 - 400

Shoreline fumigation in the thermal internal boundary layer under sea breeze conditions is a major feature of the air pollution meteorology in Kwinana region, about 30 km south of Perth in Western Australia. This region is the center of the most significant heavy industry complex in Western Australia. The area includes a power station, oil, aluminium ore and nickel refineries, and industries involved in the production of iron and steel, fertilizers and chemicals. Therefore, it is a major source of atmospheric pollutants (Young and Lynch, 1987).

The present paper describes the results of LIDAR measurements of the smoke plume for four days. This study provided an opportunity to study smoke plume dispersion in the thermal internal boundary layer at coastal region.

2. OVERVIEW OF SYNOPTIC WEATHER CONDITIONS

A good range of sea breeze conditions was covered during the study. On January 26, 1995 there was NW flow ahead of the sea breeze which commenced at the coast at about 1230 WST, was fully established from the SW by 1330 WST and turned more S throughout the afternoon. January 27 was unusual in that the sea breeze was from NW from about 1100 WST and retained a N component throughout the day. There was a cool change overnight and on January 28 the flow was a steady SW synoptic flow all day. By January 29, the flow ahead of the sea breeze was SE, and the sea breeze onset at 1000 LST was early and from SSW. Lidar operations commenced at 1100 WST and continued through to 1500 WST. This was a day with neutrally stratified sea breeze flow up to about 1000 m, rapid growth of the TIBL and consequent fumigation of both power station plumes. January 30 was a similar day with an early SSW sea breeze. Observations included the transition phase and continued through to 1600 WST.

On January 31, the early stages were particularly interesting, showing strong shear across the TIBL at about plume height. February 1 was a rest day. The sea breeze onset on February 2 was at about 1100 WST from the SSW after a SSE flow in the morning. Stratification was weak with a resulting deep TIBL and fumigation of both stacks. At 1500 WST the boundary layer appeared to be fully convective. It was similar on February 3. There was again a cool change overnight and no operations were carried out in the SW synoptic flow on February 4. On 5 and 6, it was more typical summertime condition with strong hot E flows preceding late sea breezes from SSW. The onshore flow was significantly stable, the TIBL was shallow with stage A fumigation, and Stage C fumigation was above the TIBL. Again there was strong shear across the top of the TIBL. On February 7, the sea breeze was confined to a S flow along the coast and operations were closed down (Sawford *et. al.*, 1996). Surface weather charts during the study period are presented in Figure 1.

3. LIDAR OPERATION

The smoke plume dispersions were investigated with LIDAR of the Division of Atmospheric Research CSIRO. The LIDAR was located at an alititude of about 25 m above mean sea level at the Fremantle Port Authority beacon for the Callisa Channel (Figure 2). Details of the LIDAR system are summarized in Table 2.

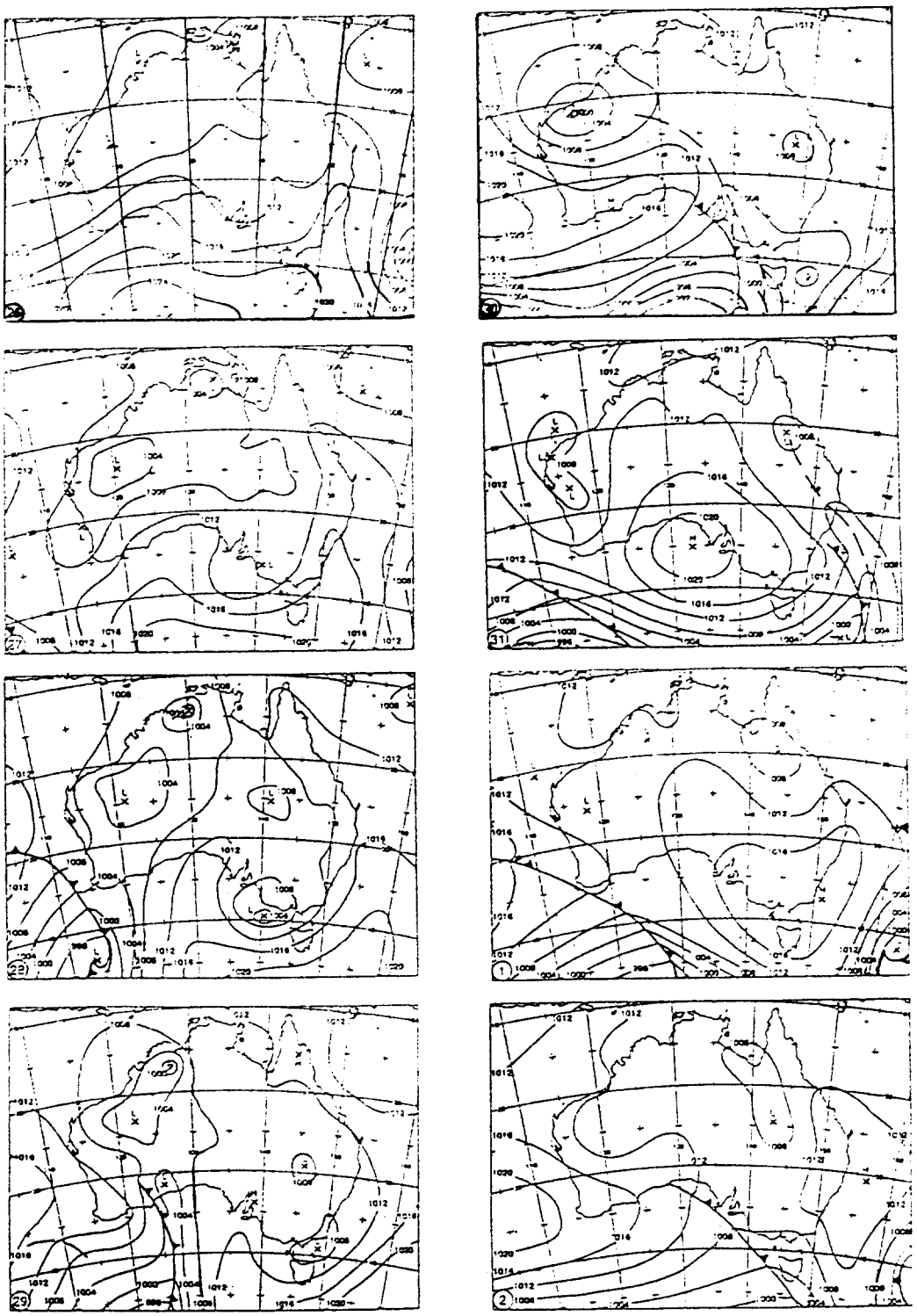

Figure 1. Daily surface weather maps from January 26 to February 2, 1995 at 0000 UTC.

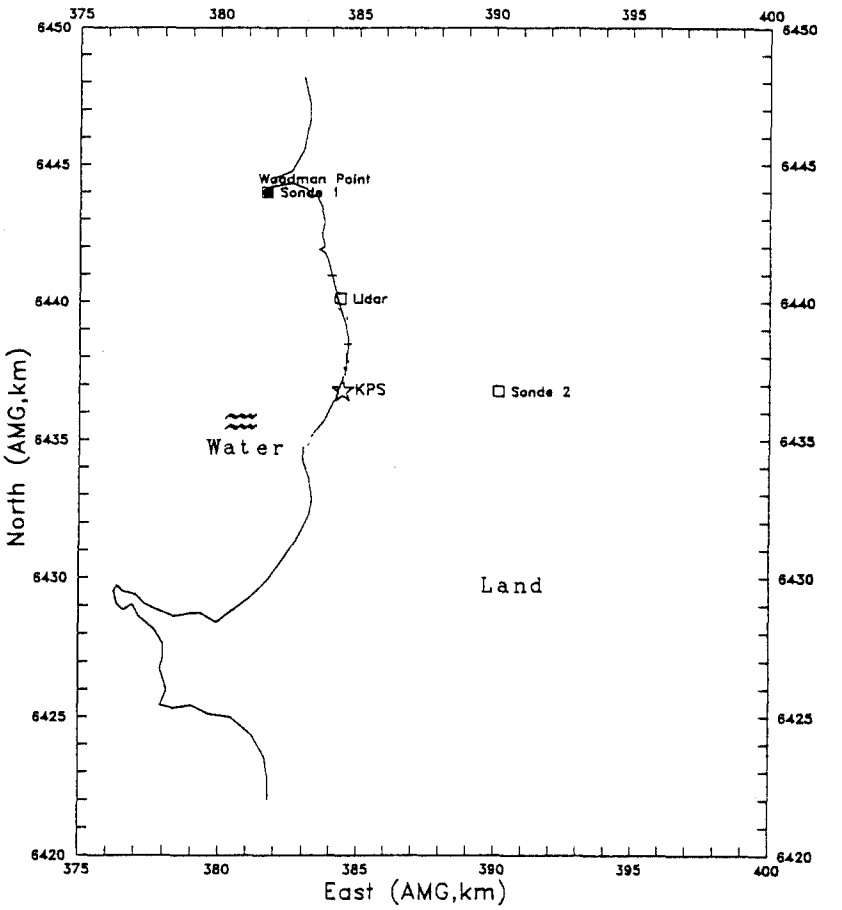

Figure 2. Location map for the study: Kwinana Power Station (KPS) and LIDAR site (Lidar) are shown.

Table 2. Parameters of LIDAR system

Measurement Technique	Incoherent backscatter
Constituents Measured	Clouds, Plume dispersion, stratosphere
Measurement Range	0.1 - 40 km
Vertical Resolution	1.5 m - 15 m(clouds); 60 m(stratosphere)
Laser Type	Nd:YAG
Wavelength	532, 355(planned 1064) nm
Pulse Repetition	10 pps
Laser Energy	0.35 J(1064), 0.15 J(532), 0.05 J(355)
Platform	Ground-based, mobile caravan
Receiver Size and Configuration	30 cm Cassegrain
Receiver Field-of-View	2 - 10 mrad
Receiver Bandwidth	1 nm
Detectors Used	2 x EMI 9816BM(S20 photocathode)
Signal Processing	Analog
Analog-To-Digital Converter	Tektronics RTD 710A, dual-channel, 10-bit digitizer

3.1 Equipment and methods

The heart of the LIDAR system is a Neodymium-doped Yttrium-aluminum- garnet (Nd:YAG) laser operating at a fundamental wavelength of 1064 nm, with harmonics of 532 nm and 355 nm. For these experiments the third harmonic was used because the UV wavelength at 355 nm is eye safe beyond about 50 m. The laser fires a pulse of light 6 ns in duration (about 1.8 m long) and with an energy (at the third harmonic) of about 70 mJ. This pulse subsequently scattered and absorbed by both air molecules and particles in the atmosphere. A small fraction of the laser beam is scattered back to the LIDAR, collected by a telescope and detected by a photo-multiplier tube. The intensity of the signal as a function of time is a measure of the particle concentration as a function of distance along the line of the laser shot.

Measurements of the smoke plume cross section were made by scanning the LIDAR in vertical planes that intersected the plume. Each scan of the plume consists of a sequence of shots at approximately 0.2° increments in elevation. Each shot is set up to sample a fixed range in the atmosphere.

3.2 Analysis procedure

The returned signal from a LIDAR pulse is given by the equation (Hoff and Froude, 1979):

$$P_r = P_0 A_r(R) \exp\left[-2\int_0^R \alpha(R)dR\right]\beta_\pi(R)\frac{l}{R^2} + kN_\lambda, \tag{1}$$

where,

R = range from the LIDAR,

P_r, P_0 = returned and output powers, respectively,

$A_r(R)$ = effective receiver area (includes solid angles, receiver efficiency and beam-receiver convergence factor),

$\beta_\pi(R)$ = molecular plus aerosol back-scatter coefficient,

$\alpha(R)$ = molecular plus aerosol extinction coefficient,

l = laser pulse spatial extent, and

kN_λ = stray light and dark current term for low levels of returned signal power.

The exponential term in Eq. (1) accounts for the attenuation of the laser pulse to and from the target. This term will reflect the turbidity of the intervening atmosphere between the LIDAR and the plume plus the attenuation of the laser pulse by the plume itself. It has

been common in plume dispersion studies to consider the effect of turbidity small and to let this term be unity (Johnson and Uthe, 1971; Uthe and Johnson, 1976). Otherwise, to do requires an assumption of the relationship between $\alpha(R)$ and $\beta_\pi(R)$ and an iterative solution of the LIDAR equation to be carried out. The calculated signal, S, then becomes:

$$S = R^2(P_r - kN_\lambda) = P_0 A_r l \beta_\pi(R). \tag{2}$$

The LIDAR raw data were analysed to produce horizontal and vertical dispersion parameters σ_y and σ_z using techniques similar to those used by Hoff and Froude (1979). Each scan through the plume is analysis for the horizontal and vertical moments of the concentration distribution. In this technique the signal $S_{i,j}$ is known at discrete digitization increments, i, in slant range for shot j at elevation angles ϕ giving:

$$M_{y,n} = \sum_{j=1}^{N} \sum_{i=1}^{I} S_{i,j} R_i^2 y_i^n / \sum_{j=1}^{N} \sum_{i=1}^{I} S_{i,j} R_i^2, \tag{3}$$

$$M_{z,n} = \sum_{j=1}^{N} \sum_{i=1}^{I} S_{i,j} R_i^2 z_i^n / \sum_{j=1}^{N} \sum_{i=1}^{I} S_{i,j} R_i^2, \tag{4}$$

where

$M_{y,n}$ = horizontal moment,

$M_{z,n}$ = vertical moment,

n = moment number of distribution,

N = number of shots in a scan,

I = number of data points,

$y_i = i\cos(\phi_j)l$,

$z_i = i\sin(\phi_j)l$, and

R_i = range = $i\,l$.

The range squared term is weighting factor to normalize the density of data points in space and it is distinct from the $1/R^2$ scaling of the LIDAR signal itself. Then, the relevant dispersion parameters are obtained from

$M_{y,1} = \bar{y} \equiv y_{cog}$; horizontal center of mass,

$M_{z,1} = \bar{z} \equiv z_{cog}$; vertical center of mass,

$\sigma_y = (M_{y,2} - \overline{y^2})^{1/2}$; horizontal dispersion coefficient, and

$\sigma_z = (M_{z,2} - \overline{z^2})^{1/2}$; vertical dispersion coefficient.

The centers of mass of the distribution are analyzed for plume bearing and rise as a function of downwind distance. σ_y and σ_z describe the spread of the plume and the last two statistics can be used to describe shear effects and peakness of the distribution. Because the plume is rarely perpendicular to the LIDAR scanning plane, the apparent horizontal dispersion coefficient will be greater than the true value. This error is corrected by some researchers by multiplying by the cosine of the angle between the plume bearing and the scanning plane (Young and Lynch, 1987).

4. EXPERIMENTAL RESULTS

Each scan of the plume consists of shots at approximately 0.2° increments in elevation. Each shot is set up to sample a fixed range in the atmosphere. Software was set up to calculate smoke plume parameters from the back-scatter data: parameters calculated include downwind distance, center of mass, σ_y, σ_z, and plume heading angle. Figure 3 shows a series of smoke plume scan.

Over 56,100 shots or laser firings during four days, *i.e.* on January 26, 30, 31, and February 2, 1995, yielded 719 scans for the various azimuth angles (usually seven to nine) which were combined to obtain 16 series "one-hour" averaged both stages A and C. Because of the finite time to complete, a scan for each azimuth angle, the "one-hour" averages varied between 45 and 73 min, and more appropriately one finds that the number of scans (usually four to nine) determines the averaging period.

Tables 3 and 4 list the principal plume parameters from the averaged data for stages A and C. The contrast between the plumes from the two stacks is remarkable. For the taller stack, Stage C (189 m), there is relatively little scatter in the hourly-mean plume height from repeated scans at any given azimuth angle, and this scatter is fairly uniform over the range of distances covered. On the other hand, for Stage A (114 m), at the first couple of downwind locations, the scatter in z is comparable with that for Stage C, and the plume is clearly rising due to its buoyancy. Clearly the lower smoke plume has encountered the TIBL and has been thereafter strongly influenced by the convective turbulence in the TIBL. The dispersion of the smoke plumes in the horizontal and vertical are also different for the two plumes.

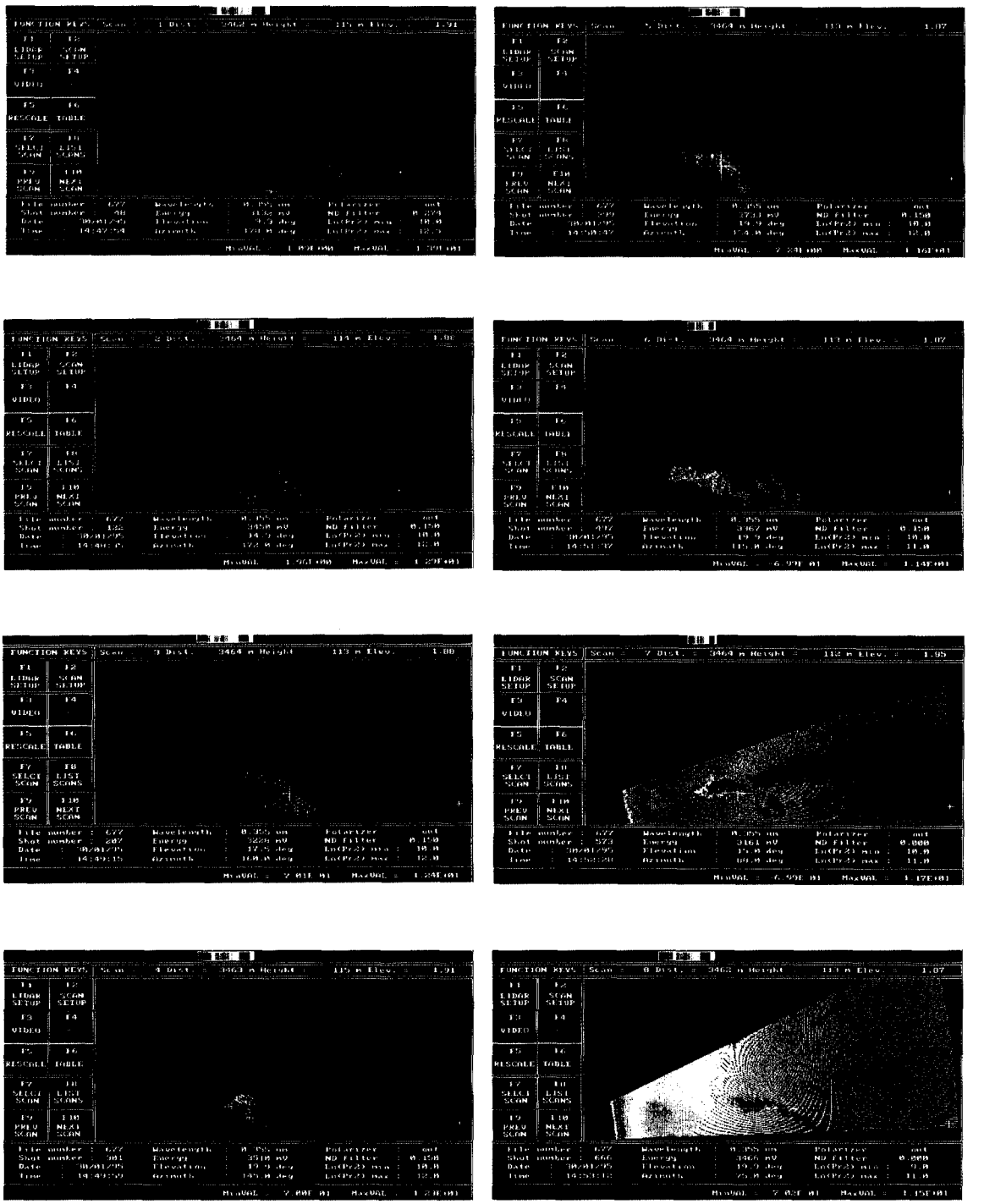

Figure 3. A series of LIDAR scans showing smoke plume.

Table 3. Hourly averaged plume dispersion results for various azimuth angle in Stage A

Series 1 (14:01:02-14:56:25 WST 26/01/95; No. of scan = 43)

Azimuth angle(deg.)	Downwind distance	Center of mass for y	Center of mass for z	σ_y	σ_z	Plume heading angle
178.4	294	3179	102	8	6	196
177.4	365	3124	117	14	9	201
172.3	724	2867	169	33	18	211
167.4	1045	2633	229	47	35	215
156.5	1769	2363	221	142	40	218
127.4	2754	2176	187	68	38	219
112.4	3343	2278	181	87	38	219

Series 2 (16:17:27-17:15:35 WST 26/01/95; No. of scan = 42)

Azimuth angle(deg.)	Downwind distance	Center of mass for y	Center of mass for z	σ_y	σ_z	Plume heading angle
177.4	509	2970	134	49	20	194
172.3	1081	2450	206	78	37	196
156.4	2135	1543	196	107	27	197
112.4	3197	1209	208	68	25	200
87.4	3761	1335	200	87	38	201
72.4	4242	1627	196	139	44	201
67.4	4463	1793	201	160	53	202
47.4	5273	2272	205	170	46	199

Series 3 (11:47:29-12:47:04 WST 30/01/95; No. of scan = 51)

Azimuth angle(deg.)	Downwind distance	Center of mass for y	Center of mass for z	σ_y	σ_z	Plume heading angle
175.4	409	3067	162	15	13	194
169.4	751	2830	200	34	30	211
157.4	1351	2593	240	71	43	221
142.4	2016	2481	205	108	58	225
131.4	2494	2533	172	159	62	227
112.4	3391	2676	160	268	67	226
85.4	4751	3147	161	207	75	223

Table 3. (continued)

Series 4 (14:07:36-15:13:14 WST 30/01/95; No. of scan = 49)

Azimuth angle(deg.)	Downwind distance	Center of mass for y	Center of mass for z	σ_y	σ_z	Plume heading angle
175.4	509	2962	157	29	20	191
169.4	967	2584	198	51	37	202
157.4	1659	2084	239	105	62	205
142.4	2277	1711	267	113	54	206
131.4	2603	1630	228	134	70	207
112.4	3137	1629	208	153	73	208
85.4	3953	1801	220	199	78	207
72.4	4511	2259	253	312	72	207
57.4	5434	2305	237	326	56	207

Series 5 (15:14:36-16:13:15 WST 30/01/95; No. of scan = 52)

Azimuth angle(deg.)	Downwind distance	Center of mass for y	Center of mass for z	σ_y	σ_z	Plume heading angle
175.4	535	2936	167	30	17	190
169.4	999	2548	201	63	30	200
157.4	1720	2001	235	131	65	202
142.4	2339	1591	251	178	67	203
131.4	2652	1487	230	166	66	204
112.4	3134	1481	200	210	64	205
85.4	3885	1655	222	296	69	205
72.4	4293	1829	240	261	67	204
57.4	5083	2366	230	380	62	204

Series 6(11:12:19-11:54:08 WST 31/01/95; No. of scan = 42)

Azimuth angle(deg.)	Downwind distance	Center of mass for y	Center of mass for z	σ_y	σ_z	Plume heading angle
175.4	479	2993	159	24	14	191
169.4	917	2642	201	63	24	203
157.4	1575	2206	195	122	30	208
142.4	2190	1897	186	124	39	209
131.4	2549	1833	161	188	50	211
112.4	3154	1834	153	239	51	211
85.4	4090	2072	172	263	47	210
72.4	4744	2479	188	287	42	210

Table 3. (continued)

Series 7(13:07:23-13:54:41 WST 31/01/95; No. of scan = 54)

Azimuth angle(deg.)	Downwind distance	Center of mass for y	Center of mass for z	σ_y	σ_z	Plume heading angle
175.4	526	2945	161	29	14	190
169.4	977	2573	207	48	29	201
157.4	1650	2097	226	93	41	206
142.4	2209	1858	206	121	53	209
131.4	2568	1756	187	158	60	210
112.4	3144	1714	174	176	52	210
85.4	4091	2072	188	244	67	211
72.4	4685	2393	219	261	57	210
57.4	5784	3223	216	257	68	209

Series 8(14:16:19-15:12:22 WST 31/01/95; No. of scan = 54)

Azimuth angle(deg.)	Downwind distance	Center of mass for y	Center of mass for z	σ_y	σ_z	Plume heading angle
175.4	488	2984	157	22	16	191
169.4	912	2648	192	53	30	203
157.4	1588	2187	227	70	41	208
142.4	2177	1915	267	132	57	210
131.4	2652	1798	221	155	67	210
112.4	3147	1783	222	176	65	211
85.4	4103	2093	233	215	72	210
72.4	4817	2579	242	294	64	211
57.4	5931	3395	245	318	68	210

Series 9(15:17:08-16:06:47 WST 31/01/95; No. of scan = 67)

Azimuth angle(deg.)	Downwind distance	Center of mass for y	Center of mass for z	σ_y	σ_z	Plume heading angle
175.4	521	2949	183	22	15	190
169.4	974	2580	215	49	36	202
157.4	1627	2143	238	85	47	207
142.4	2210	1858	238	127	71	209
131.4	2561	1787	233	160	71	210
112.4	3146	1753	217	171	69	210
85.4	4070	2032	225	240	66	210
72.4	4725	2450	236	312	65	210
57.4	5880	3335	250	350	71	210

Table 3. (continued)

Series 10(13:07:35-14:00:19 WST 02/02/95: No. of scan = 44)

Azimuth angle(deg.)	Downwind distance	Center of mass for y	Center of mass for z	σ_y	σ_z	Plume heading angle
175.4	499	2973	141	18	15	191
169.4	908	2652	170	34	29	203
157.4	1573	2208	203	42	43	209
142.4	2182	1915	262	71	58	210
131.4	2547	1837	226	81	67	211
112.4	3152	1826	232	102	42	211
85.4	4170	2220	215	144	74	212
72.4	4884	2673	238	180	71	212
57.4	6065	3548	253	239	59	211

Series 11(15:06:15-16:03:07 WST 02/02/95: No. of scan = 54)

Azimuth angle(deg.)	Downwind distance	Center of mass for y	Center of mass for z	σ_y	σ_z	Plume heading angle
175.4	549	2905	147	24	17	190
169.4	1028	2516	181	42	31	202
157.4	1654	2043	216	51	47	206
142.4	2242	1779	228	60	61	206
131.4	2617	1625	245	66	71	207
112.4	3142	1657	243	79	78	208
85.4	4078	2089	300	177	98	210
72.4	4695	2520	322	262	128	210
57.4	5762	3193	330	254	114	208

Table 4. The same as in Table 3 except for in Stage C

Series 1(15:01:01-16:14:46 WST 26/01/95: No. of scan = 41)

Azimuth angle(deg.)	Downwind distance	Center of mass for y	Center of mass for z	σ_y	σ_z	Plume heading angle
177.4	405	3080	220	29	17	199
172.3	916	2636	253	65	35	202
167.4	1231	2400	315	114	44	205
156.5	1886	1886	286	84	47	203
127.4	2775	1687	290	114	32	209
112.4	3204	1524	229	99	33	206
87.4	3974	1810	223	138	39	206
72.4	4470	1875	211	170	49	205
67.4	4723	2154	247	173	35	205
47.4	6435	3571	252	187	40	204

Table 4. (continued)

Series 2(13:07:09-14:06:00 WST 30/01/95: No. of scan = 36)

Azimuth angle(deg.)	Downwind distance	Center of mass for y	Center of mass for z	σ_y	σ_z	Plume heading angle
175.4	484	2987	262	41	21	200
169.4	1006	2540	307	74	36	200
157.4	1680	2054	334	104	41	204
142.4	2256	1753	314	106	32	207
131.4	2597	1648	301	120	36	207
112.4	3136	1612	276	149	46	208
85.4	3999	1860	309	163	33	208
72.4	4580	2242	314	198	44	208
47.4	7138	4410	276	330	43	208

Series 3(12:06:01-12:44:31 WST 31/01/95: No. of scan = 45)

Azimuth angle(deg.)	Downwind distance	Center of mass for y	Center of mass for z	σ_y	σ_z	Plume heading angle
175.4	568	2902	277	56	20	189
169.4	1077	2460	289	78	22	198
157.4	1773	1927	298	93	24	202
142.4	2304	1660	295	95	25	205
131.4	2625	1561	277	95	26	205
112.4	3135	1532	270	88	27	206
85.4	3968	1827	263	107	41	207
72.4	4479	2088	270	157	35	207
57.4	5575	2973	264	241	33	207

Series 4(14:06:01-14:44:31 WST 02/02/95: No. of scan = 45)

Azimuth angle(deg.)	Downwind distance	Center of mass for y	Center of mass for z	σ_y	σ_z	Plume heading angle
175.4	450	3024	228	23	16	192
169.4	896	2666	231	31	26	204
157.4	1546	2249	279	53	37	209
142.4	2160	1969	278	55	40	211
131.4	2540	1872	242	61	44	211
112.4	3157	1849	232	91	75	211
85.4	4197	2135	232	144	87	211
72.4	4935	2742	266	198	84	212
57.4	6303	3820	244	222	94	212

5. SUMMARY AND CONCLUSIONS

The Kwinana Shoreline Fumigation Experiment(KSFE) took place at Fremantle, WA, Australia between January 23 and February 8, 1995. Smoke plumes from power station stacks have been tracked at various azimuth angle with LIDAR. Over 56,100 shots or laser firing during four days, *i.e.* on January 26, 30, and 31 and February 2 , yielded 719 scans for the various azimuth angles(usually seven to nine) which were combined to obtain 16 series "one-hour" averaged both stages A and C. Because of the finite time to complete a scan for the each azimuth angle the "one-hour" averages varied between 45 and 73 min and more appropriately one finds that the number of scans(usually four to nine) determines the averaging period.

The use of a LIDAR when coupled to a method to directly extract dispersion statistics from the data has been shown to yield useful analytical capabilities for air pollution dispersion estimates. The contrast between the plumes from the two stacks is remarkable.

The large heights of the stacks and their proximity to the coast lead to different plume dispersion behavior depending on the nature of the TIBL. During stable onshore winds when the plumes were emitted directly into the stable air above the TIBL, the plumes experience relatively little dispersion until they encounter the TIBL, often several kilometers downwind of the stacks.

ACKNOWLEDGEMENTS

The author would like to thank Dr. S. A. Young and Mr. G. Patterson of CSIRO DAR for the help of LIDAR data analysis. This paper was supported by NON DIRECTED RESEARCH FUND, Korea Research Foundation, 1996.

REFERENCES

Hoff, R. M., and F. A. Froude, LIDAR observation of plume dispersion in northern Alberta. *Atmos. Environ.*, 13, 35-43, 1979.

Johnson, W. B., and E. E. Uthe, LIDAR study of the Keystone stack plume. *Atmos. Environ.*, 5, 703-724, 1971.

Manins, P. C., Kwinana Power Station SO_2 Study: A Report to State Energy Commission of Western Australia, CSIRO Division of Atmospheric Research, Aspendale, Australia, 1990.

Sawford, B. L., A. K. Luhar, J. A Noonan, I. H. Yoon, S. A. Young, W. L. Physick, G. R. Patterson, J. M. Hacker, J. N. Carras, D. J. Williams and A. Blockley, Shoreline Fumigation at Kwinana: A Study to Assess, Validate and Improve DISPMOD. Final Report SB/1/227, CSIRO Division of Atmospheric Research, Aspendale, Australia, 1996.

Uthe, E. E. and W. B. Johnson, Lidar Observation of Plume Diffusion at Rancho Seco Generating Station, EPRI Report NP-238 (SOA 75-316), Palo Alto, CA., U.S.A., 1976.

Young, S. A., and M. J. Lynch, LIDAR observations of smoke plume dispersion from tall stacks in a coastal environment. *Clean Air* 21(1), 25-30, 1987.